Surface hopping, transition state theory, and decoherence. II. Thermal rate constants and detailed balance

Amber Jain and Joseph E. Subotnik

Citation: The Journal of Chemical Physics **143**, 134107 (2015); doi: 10.1063/1.4930549
View online: http://dx.doi.org/10.1063/1.4930549
View Table of Contents: http://scitation.aip.org/content/aip/journal/jcp/143/13?ver=pdfcov
Published by the AIP Publishing

Surface hopping, transition state theory, and decoherence. II. Thermal rate constants and detailed balance

Amber Jain and Joseph E. Subotnik[a)]
Department of Chemistry, University of Pennsylvania, 231 South 34th Street, Philadelphia, Pennsylvania 19104, USA

(Received 17 June 2015; accepted 27 August 2015; published online 2 October 2015)

We investigate a simple approach to compute a non-adiabatic thermal rate constant using the fewest switches surface hopping (FSSH) dynamics. We study the effects of both decoherence (using our augmented-FSSH (A-FSSH) algorithm) and forbidden hops over a large range of parameters, including high and low friction regimes, and weak and strong electronic coupling regimes. Furthermore, when possible, we benchmark our results against exact hierarchy equations of motion results, where we usually find a maximum error of roughly a factor of two (at reasonably large temperatures). In agreement with Hammes-Schiffer and Tully, we find that a merger of transition state theory and surface hopping can be both accurate and efficient when performed correctly. We further show that detailed balance is followed approximately by A-FSSH dynamics. © *2015 AIP Publishing LLC.* [http://dx.doi.org/10.1063/1.4930549]

I. INTRODUCTION

Nonadiabatic transitions come in all flavors in the condensed phase. On the one hand, many nonadiabatic processes are short-lived and downhill in energy, e.g., photoinduced dynamics. On the other hand, going all the way to back the famous ion exchange processes studied by Marcus,[1] there are many nonadiabatic processes that span long periods of time, with large thermal barriers. While the former processes can be treated with direct surface hopping dynamics (which is popular nowadays),[2–6] obviously the latter processes will require some tricks of statistical mechanics if one is interested in a thermal rate constant. Direct dynamics would take too much computational time and one would not learn very much while waiting.

Unfortunately, a straightforward extension of the classical transition state theory[7–10] (TST) to include non-adiabatic effects is challenging if we insist on treating classical and quantum degrees of freedom at different levels of theory (as in surface hopping).[11–15] That being said, the problem of calculating rate constants and rare event passages with surface hopping is not new, and Hammes-Schiffer and Tully (HST) long ago developed a method to combine fewest switches surface hopping (FSSH) and TST.[16] In their approach, classical TST is generalized to include a Boltzmann average of the contributions to the rate constant from various adiabatic surfaces, and trajectories are initialized at the dividing surface. The initial quantum amplitudes, an essential ingredient in the surface hopping algorithm, are computed by backward-propagating trajectories in time using a fictitious surface hopping approach. Subsequently, a weighting factor is used to correct for the errors introduced due to the fictitious (backwards) hopping algorithm. Finally, armed with the initial quantum amplitudes, the trajectories are propagated forwards in time using the regular surface hopping method to compute the transmission coefficient. References 16–24 show that this algorithm can be used successfully to calculate rate constants for various processes.

Given the published success of the HST scheme at reproducing rate constants with surface hopping, our goal in this paper is to study some aspects regarding the intersection of nonadiabatic dynamics and TST that, to our knowledge, have not yet been addressed in the literature. As a generic tool for nonadiabatic dynamics, surface hopping has a very long and rich history, but there are many nuances that arise in the surface hopping algorithm: e.g., detailed balance, frustrated hops, and decoherence effects. Thus far, however, these nuances have not been fully analyzed in the context of a TST rate theory. Recent work suggests that decoherence[25–30] can have a significant effect. Furthermore, modern advances in exact quantum methodologies[31–34] now allow us to study long time processes and rate constants over a wide range of system-bath couplings (all the way from the nonadiabatic regime to the adiabatic regime). Thus, a systematic comparison of TST-FSSH rate constants with exact quantum data would appear timely.

In what follows below, we will make such a comparison using a TST-FSSH theory that is very similar to the HST approach, with just two differences. These difference are the following: first, we use an approximate and simplified scheme for backward-propagation. In brief, the trajectories are back-evolved solely on one adiabatic surface (see Sec. II C 1). This modification was applied because of our interest in a purely Markovian algorithm. This scheme has been applied previously[35] (in Paper I) to compute transmission coefficients for scattering processes using surface-hopping trajectories that start at a transition state geometry. Second, compared with HST, we employ a slightly different definition for the semiclassical TST weightings — each trajectory is weighted on a single adiabatic surface only. (The rationale for this modification is explored in Sec. V B.) Using this simple protocol, we have several objectives for this paper.

a)Electronic address: subotnik@sas.upenn.edu

1. Our first objective is to benchmark TST surface hopping rates constants vs (i) direct surface hopping rate constants (for lower barriers, when possible) and (ii) exact hierarchy equations of motion (HEOM) calculations. In so doing, we want to establish whether TST surface hopping is accurate over a range of dynamical regimes and, if not, assess what is the source of any errors. This objective is in the same spirit as Ref. 24.
2. Our second objective is to examine the exact dependence of a TST-FSSH rate constant on the location of the dividing surface. Exact rate theory is independent of the choice of the dividing surface[11] and, in practice, the utility of a TST-FSSH rate constant will be limited if the answer depends sensitively on the dividing surface.
3. Formally, one can show that detailed balance is one consequence of time-reversibility.[36] Even though surface hopping is not time-reversible,[37] in Paper I, we have shown that scattering transmission coefficients do approximately obeyed detailed balance (after averaging over initial energy). Furthermore, there is a great deal of accumulated evidence that direct FSSH dynamics do recover detailed balance approximately.[38,39] With this in mind, our third objective is to investigate if detailed balance is correctly satisfied by TST-FSSH. In practice, for detailed balance to hold, the transmission coefficient κ must be identical for the forward and reverse reactions, and we will check numerically whether or not $\kappa_{l\to r} = \kappa_{r\to l}$.
4. Our fourth objective is to determine the effects of decoherence on thermal rate constants. As we have mentioned above, the overcoherence problem can have large effects and cannot be ignored.[28,29] To examine decoherence effects, we will employ the augmented-FSSH (A-FSSH)[30] algorithm which applies a decoherence correction. We showed in Paper I that, without any decoherence effects, FSSH transmission coefficients are smaller by a factor of two compared to the exact results for the case of weak electronic coupling — whereas, A-FSSH transmission coefficients are nearly exact (for high enough temperatures). Furthermore, we would also like to identify those regimes where the effects of decoherence are important and those regimes where these effects are not important.[40]
5. Forbidden hops are an inevitable, but awkward, component of the Tully FSSH scheme. On the one hand, forbidden hops are essential in surface hopping, for they are the key ingredients that allows FSSH to achieve detailed balance.[38,41] On the other hand, the presence of forbidden hops erases some of the symmetry between amplitudes and surfaces in the FSSH algorithm, which can lead to problems.[5] To date, a great deal of the literature has discussed the treatment of forbidden hops and various protocols have been suggested.[5,42–45] Jasper and Truhlar have performed probably the most extensive calculations.[46–49] To our knowledge, thus far, no one has assessed the affect of forbidden hops on the dynamics of thermally activated rare event processes and our fifth objective is to investigate that very effect.
6. Formally, the velocity distribution at the transition state is a separate, Boltzmann distribution only according to classical dynamics on one (adiabatic) surface. For a nonadiabatic dynamics problem, even with classical nuclei, there need not be such an assumption in general—and indeed, such an assumption might not appear compatible with FSSH dynamics where there is velocity rescaling. As such, the sixth and final objective of this paper is to investigate the role of velocity initialization on the form of a TST rate constant. In particular, what are the implications of how one chooses such an initial set of velocities in a condensed phase, and how can one pick out the optimal initial set?

These are our six objectives. Finally, before reporting on any theory or results, we should mention that there is a very different surface-hopping approach (by Zhao, Li, Zheng, and Liang)[50] for computing hopping probabilities between diabats based on Zhu-Nakamura (ZN) theory[51] (rather than Tully dynamics). The Zhao approach avoids the problem of initialization of quantum amplitudes from backwards propagation and captures some of the important tunneling effects by including non-vertical hops. While the Zhao approach relies on the assumption of independent crossings (and thus complete decoherence whenever the trajectories leave the curve-crossing region), Refs. 50 and 52 show that the method can be used to treat (at least come cases of) dynamics with strong friction. Future work will no doubt explore the above mentioned questions in the context of the Zhao algorithm, as well as the feasibility of on-the-fly dynamics (with *ab initio* electronic structure theory).

An outline of the paper is as follows: In Sec. II, the various methods to compute rate constants are described. This includes a direct computation of the rate constant, as well as the TST-like approaches. The model system studied and the computational details are given in Sec. III and the results are presented and discussed in Secs. IV and V, respectively. Section VI concludes the paper.

II. METHODS

Henceforward, we limit our discussion to a two level system, with the adiabatic potential energy surfaces given by $V_{1/2}$ (though what follows can be generalized for multiple energy surfaces). We will consider both the normal and the inverted regimes, which are schematically shown in Figs. 1(a) and 1(c). The reaction coordinate is s. For the normal regime, the left side of the well represents the reactants and the right side the products. In the inverted regime, the upper adiabat represents the reactant and the lower adiabat represents the products.

Rate constants can be computed either directly (in time) starting from the reactants, or using a transition state theory approach. We now describe both these methods.

A. Direct computation of rate constant

The most direct method to compute rate constants is to equilibrate a large set of trajectories in the reactant region and monitor the number of trajectories in that same reactant region while recording the decay. After a short transition time, the relaxation can be described by first-order dynamics as

$$\dot{P}_r = -k_f P_r + k_b P_p, \tag{1}$$

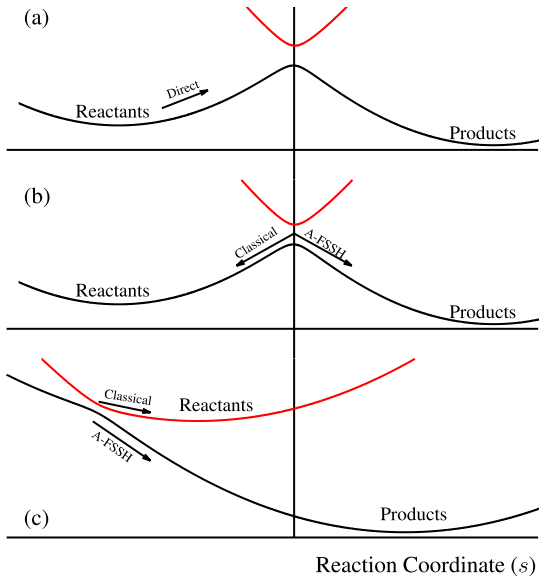

FIG. 1. Schematic view of the potential energy surfaces along the reaction coordinate s for the normal and the inverted regimes. (a) Direct approach (for normal regime): after equilibrating the system in the reactant well, we measure the decay of the population in the reactant region. (b) Transition state approach in the normal regime: trajectories are initiated near the dividing surface, back-propagation is performed using classical dynamics on the ground surface and forward propagation using A-FSSH. (c) Transition state approach in the inverted regime (for top to bottom reaction): The backward classical dynamics is performed on the upper adiabat, followed by forward propagation using A-FSSH.

where P_r and P_p are the reactant and the product populations, respectively, and k_f and k_b are the forward and the backward rate constants, respectively. Fitting the long time dynamics to an exponential gives the total rate constant $k = k_f + k_b$, and k_f can be computed using

$$k_f = k\frac{1}{1+e^{-\beta\epsilon}}, \tag{2}$$

where $\beta = 1/k_B T$, T is the temperature, and ϵ is the reaction energy.

Using Eq. (2), we can extract rate constants for both the adiabatic and non-adiabatic reactions. For adiabatic dynamics, straightforward classical dynamics can be run. For non-adiabatic dynamics, we will utilize our A-FSSH approach that includes decoherence effects without significant addition to the computational cost. A-FSSH has been used previously with success to compute rate constants directly.[29,53,54] The details of the A-FSSH algorithm are described in detail in the Appendix A of Paper I (which closely follows the details of Ref. 29).

B. Transition state formalism — classical

The cost of direct dynamics is prohibitive for reactions with large barriers. As such, the reactive flux approach presents a practical and accurate alternative. Before describing the formalism to account for the non-adiabatic effects, which is the main focus of this paper, we review how to compute the rate constant on a single energy surface (in the normal regime). In the reactive flux approach, the rate constant is given by[55]

$$k = \frac{\langle \delta(s) v_s h[s(t_P)]\rangle}{\langle 1 - h[s]\rangle}, \tag{3}$$

where v_s is the velocity along s, h is the Heaviside step function that projects onto the products side $s > 0$, t_P is the plateau time, and $Z_r = \langle 1 - h[s]\rangle$ is the reactant partition function. The angular brackets denote a thermodynamic average

$$\langle(\ldots)\rangle = \frac{1}{Z}\int d\mathbf{P} e^{-\beta\sum_i P_i^2/2m_i}\int d\mathbf{Q} e^{-\beta V(\mathbf{Q})}(\ldots), \tag{4}$$

where the coordinates and the momenta of the whole system are $\mathbf{Q}$ and $\mathbf{P}$, respectively, and $V(\mathbf{Q})$ is the potential energy function. Here, Z is the partition function of the total system.

The above rate constant can be re-written as

$$k = k_{TST}\kappa, \tag{5}$$

with

$$k_{TST} = \frac{\langle \delta(s) v_s h[v_s]\rangle}{\langle 1 - h[s]\rangle}, \tag{6}$$

and

$$\kappa = \frac{\langle \delta(s) v_s h[s(t_P)]\rangle}{\langle \delta(s) v_s h[v_s]\rangle}. \tag{7}$$

The transition state estimate for the rate constant k_{TST} assumes no re-crossing through the dividing surface, and the transmission coefficient κ accounts for the dynamical re-crossings.

In practice, κ is computed by propagating a statistically large number of trajectories at the dividing surface, with the initial configuration (positions and velocities) chosen from a Maxwell-Boltzmann distribution. In this paper, we use a variation of the Keck formalism[21,56,57]

$$\kappa = \frac{\langle \delta(s) v_s h[v_s]\alpha\rangle}{\langle \delta(s) v_s h[v_s]\rangle}, \tag{8}$$

where α is 1 if, and only if, the trajectory propagated back in time stabilizes in the reactant minima without ever re-crossing the dividing surface and the trajectory stabilizes in the product region upon forward propagation (with or without re-crossings). Otherwise, $\alpha = 0$.

C. Quantum rate constant

If we move beyond a single potential energy surface $V(\mathbf{Q})$ and address the presence of multiple energy surfaces, several obstacles arise (which we now discuss).

1. Backward propagation

The first obstacle is the necessity of back propagation. In order to initialize a trajectory at the crossing point and run dynamics, one requires *a priori* knowledge of the quantum amplitudes c_j (which are needed for computing hopping probabilities). In Paper I, we proposed an approximate method to perform this backward dynamics, and this method was benchmarked against exact scattering calculations for a one dimensional barrier. A scheme of our approach is shown in Figs. 1(b) and 1(c) for the normal and the inverted regimes,

respectively. In summary, starting at the dividing surface, with the identity matrix

$$\mathbf{U}(0) = \begin{pmatrix} 1 & 0 \\ 0 & 1 \end{pmatrix}, \tag{9}$$

backward dynamics are performed on one adiabatic surface with the time-reversed Schrödinger equation for $\mathbf{U}$,

$$i\hbar\dot{\mathbf{U}} = -\begin{pmatrix} V_1 & -i\hbar(\mathbf{P}/m).\mathbf{d_{12}} \\ i\hbar(\mathbf{P}/m).\mathbf{d_{12}} & V_2 \end{pmatrix}\mathbf{U}. \tag{10}$$

For a normal regime, one performs backwards dynamics on the ground adiabatic state [see Fig. 1(b)]; for transfer downhill through the inverted regime, one performs backward dynamics on the upper adiabatic state [see Fig. 1(c)]. Here, $V_{1/2}$ are the adiabatic potentials, $\mathbf{P}$ is the classical momentum, and $\mathbf{d_{12}}$ is the non-adiabatic coupling vector. Once the reactant basin is reached (based on some criteria, see Sec. III), the initial coefficients can now be computed as

$$c_j(0) = U^{\dagger}_{j,r}(t_R). \tag{11}$$

Here t_R is the time required for backward propagation and r is the adiabatic surface corresponding to the reactants.

Equations (9)-(11) represent an approximate version of the algorithm developed by Hammes-Schiffer and Tully.[16] In practice (as was shown in Paper I), the transmission probabilities computed using our scheme are nearly identical compared to a direct computation.

2. Transition state formalism

The second obstacle is the need for a rigorous semiclassical rate theory, given that surface hopping approaches rely on a difficult and sometimes awkward separation of quantum and classical degrees of freedom. With this in mind, there are multiple ways of generalizing Eqs. (3) and (4) to the case of multiple potential energy surfaces.[14,58,59] Our approach will follow the model of Hammes-Schiffer and Tully[16] reasonably closely. We will define a quantum-mechanical rate constant as follows:

$$k^{QM} = \frac{\langle \delta(s) v_s h[s(t_P)] \rangle_r}{\langle 1 - h[s] \rangle_r}, \tag{12}$$

with

$$\langle (\ldots) \rangle_r = \frac{1}{Z} \sum_j \int d\mathbf{P} e^{-\beta \sum_i P_i^2/2m_i} \int d\mathbf{Q} e^{-\beta V_r(\mathbf{Q})} |c_j|^2 (\ldots). \tag{13}$$

Note that Eqs. (3) and (12) are identical, but the definitions of the averages [in Eqs. (4) and (13)] are different.

Several clarifications are needed to correctly motivate this formalism.

- $V_r(\mathbf{Q})$ refers to the adiabatic potential energy surface along which backward propagation occurs (eventually to the reactant). We emphasize that, in our scheme, all trajectories are initialized with the same Boltzmann factor ($\exp(-\beta V_r)$), regardless of their active surface. We find that this uniform Boltzmann (exponential) factor is essential for obtaining a rate constant that is relatively independent of the dividing surface.
- In assigning an active surface to each trajectory at the crossing point, we weight each surface according to the $|c_j|^2$ value as obtained with back-propagation.
- Finally, the momentum is chosen by ansatz from a Boltzmann distribution that depends only on the temperature of the bath, and thus, the momentum distribution is independent of the initial adiabatic surface. While this assumption of decoupled velocities might well appear problematic (especially in the limit of the zero friction), we will show that this ansatz is important for obtaining rate constants that are approximately independent of the dividing surface over a range of frictional strengths. This decoupling is the central difference between the present paper regarding rate theory in the condensed phase (with friction) and the previous paper (Paper I) regarding transmission coefficients in the gas phase (without friction).

The main deviation between the above protocol and the HST protocol, is that Ref. 16 employs a Boltzmann average of the contribution from the various adiabatic surfaces. Thus, for e.g., in the normal regime, one finds a weight of $\exp(-\beta V_2)$ on the upper adiabat according to Ref. 16, while we weight such a trajectory with $\exp(-\beta V_1)$. This difference will be discussed in detail in Sec. V.

For purposes of interpretation only, and in the spirit of separating the classical rate constant into the transition state and transmission coefficient components, we define the analogous semiclassical transmission coefficient as follows:

$$k^{QM}_{TST} = \frac{\langle \delta(s) v_s h[v_s] \rangle_d}{\langle 1 - h[s] \rangle_r}, \tag{14}$$

$$\kappa^{QM} = \frac{\langle \delta(s) v_s h[v_s] \alpha \rangle_r}{\langle \delta(s) v_s h[v_s] \rangle_d}, \tag{15}$$

with

$$\langle (\ldots) \rangle_d = \frac{1}{Z} \int d\mathbf{P} e^{-\beta \sum_i P_i^2/2m_i} \int d\mathbf{Q} e^{-\beta V_d(\mathbf{Q})} (\ldots), \tag{16}$$

and $\langle (\ldots) \rangle_r$ is defined in Eq. (13). Here V_d is the diabatic barrier height.

In Eq. (15), α is defined in the same way as in the adiabatic case—α is 1 if and only if the backward propagation ends in the reactant region without re-crossing the dividing surface and the forward propagation ends in the product region; otherwise α is zero. This definition of α works well with our simplified version of backward-propagation along a single adiabat.

3. Forbidden hops

The third obstacle facing a nonadiabatic rate theory (via surface hopping) is the treatment of forbidden (energetically inaccessible) hops. As will be shown below, an improper treatment of forbidden hops can lead to rate constants with dramatically large errors. For our protocol below, we follow the insightful spirit of Truhlar's[48] "∇V" approach. Namely, if a frustrated hop is encountered, the velocity is reversed along the non-adiabatic coupling vector if two conditions

hold: (a) $(\mathbf{F_1}.\mathbf{d_{12}})(\mathbf{F_2}.\mathbf{d_{12}}) < 0$, where $\mathbf{F_1}$ and $\mathbf{F_2}$ are the forces on the lower and the upper adiabat, respectively, and (b) $(\mathbf{P}.\mathbf{d_{12}})(\mathbf{F_2}.\mathbf{d_{12}}) < \mathbf{0}$. Condition (a) stipulates that we reverse velocities only if the different surfaces point us in different directions; condition (b) stipulates that we reverse velocities only if the new surface opposes our current momentum. These two conditions are reasonable restrictions that limit the instances of velocity reversal; in general, we find that they have a minimal effect on almost all calculations (with the exception of some barrier crossings, as discussed below). Truhlar *et al.* suggested condition (b) long ago.[48]

D. Algorithm

For completeness, we now give a step-by-step outline of our algorithm.

1. Set $\kappa_{den} = 0$ and $\kappa_{num} = 0$. These represent the denominator and the numerator of κ in Eq. (15).
2. Initiate the coordinates ($\mathbf{Q}$) and the momenta ($\mathbf{P}$) on the dividing surface from a Maxwell-Boltzmann distribution. All velocities must have a negative projection in the direction of the reactant basin. For instance, in the normal regime of Fig. 1(b), only positive velocities are considered. Save these positions and momenta $\mathbf{Q}(0) = \mathbf{Q}$ and $\mathbf{P}(0) = \mathbf{P}$, and the velocity along the reaction coordinate $v_s(0)$. The contribution to the denominator of κ from this trajectory is $\kappa_{den} = \kappa_{den} + v_s(0)e^{-\beta V_d}$.
3. Initialize $U_{jk}(0) = \delta_{jk}$ [see Eq. (9)]. Initialize the current adiabatic surface as $\lambda = r$ where r is the adiabatic surface corresponding to the reactant basin (which must be reached with back propagation).
   (a) For the normal regime of Fig. 1(b), we set r as the ground state.
   (b) For the top to bottom reaction in the inverted regime of Fig. 1(c), we set r as the upper adiabatic state.

   During back-propagation, $\mathbf{Q}$ and $\mathbf{P}$ are evolved using classical mechanics along surface r (with no hops), and $\mathbf{U}$ is evolved using the time-dependent Schrödinger equation [see Eq. (10)]. Backward propagation continues until the trajectory reaches the reactant region. If the trajectory ever re-crosses the dividing surface during this time, terminate the trajectory and go back to step 2. Otherwise, proceed to step 4.
4. Set the variables $\mathbf{Q} = \mathbf{Q}(0)$, $\mathbf{P} = \mathbf{P}(0)$, and the moments $\delta\mathbf{Q} = 0$, $\delta\mathbf{P} = 0$. The initial quantum amplitudes are $c_j(0) = U^{\dagger}_{jr}(t_R)$, where t_R is the time required to reach the reactant region from the previous step. The initial surface $\lambda(0) = j$ is chosen with probability $|c_j(0)|^2$.
5. Evolve each trajectory forward with variables $(\mathbf{Q}, \mathbf{P}, \delta\mathbf{Q}, \delta\mathbf{P})$ using the A-FSSH algorithm[29] until the pre-defined plateau time t_P. Set $\alpha = 1$ if the trajectory stabilizes in the product region, and 0 otherwise. If $\alpha = 1$, then add $\kappa_{num} = \kappa_{num} + v_s(0)\exp(-\beta V_r(0))$, where $V_r(0)$ is the initial adiabatic potential that was employed for backward propagation.
6. Go back to step 2 and iterate until statistical convergence.

III. COMPUTATIONAL DETAILS

We now describe the model system investigated, followed by the details of the A-FSSH algorithm, the HEOM method and Straub-Berne (SB) theory.

A. Model system

We compute the rate of electron transfer for the spin-boson Hamiltonian, one of the most widely studied systems for electron transfer. In our version, the Hamiltonian consists of a two level system (representing an electron with two states) coupled to a quantum Brownian oscillator with nuclear coordinate Q_0. Formally, the Hamiltonian is

$$H = H_e + H_n + H_{en} + H_b + H_{nb} + H_{ren}, \tag{17}$$

with

$$H_e = \frac{\epsilon}{2}\sigma_z + V_c\sigma_x, \tag{18}$$

$$H_n = \frac{P_0^2}{2m_0} + \frac{1}{2}m_0\omega_0^2Q_0^2, \tag{19}$$

$$H_{en} = kQ_0\sigma_z, \tag{20}$$

$$H_b = \sum_{i=1}\left(\frac{P_i^2}{2m_i} + \frac{1}{2}m_i\omega_i^2Q_i^2\right), \tag{21}$$

$$H_{nb} = \sum_{i=1} d_iQ_iQ_0, \tag{22}$$

$$H_{ren} = \sum_{i=1}\frac{d_i^2}{2m_i\omega_i^2}Q_0^2. \tag{23}$$

Here, σ_z and σ_x are the Pauli matrices. The driving force is given by ϵ, V_c is the diabatic coupling, and the coupling k is a function of the reorganization energy λ, $k = \sqrt{0.5\lambda m_0\omega_0^2}$. The reaction coordinate Q_0 is further coupled to a harmonic bath with masses m_i, coordinates Q_i, momenta P_i, and frequency ω_i. The couplings d_i are described by the spectral density,

$$J(\omega) = \frac{\pi}{2}\sum_i\frac{d_i^2}{m_i\omega_i}\delta(\omega - \omega_i). \tag{24}$$

In this work, we employ the continuous Ohmic form for the spectral density $J(\omega) = \eta\omega$, where η is the damping coefficient.

In practice, as is well known, one can integrate out the harmonic bath (with the coupling given by the Ohmic spectral density) and thereupon, one finds a system (with two levels and one harmonic oscillator) subject to a random force.[60] The resulting dynamics can be simulated by obtaining forces from the Langevin equation,

$$\mathbf{F} = -\nabla E_\lambda - \eta\mathbf{P} + \zeta, \tag{25}$$

where E_λ is the active adiabatic potential energy surface and ζ are the random forces chosen from a Gaussian distribution with the standard deviation $\sigma = \sqrt{2\eta m_0k_BT/dt}$. dt is the integration time step.[61]

We investigate both the normal and inverted regimes. The parameters of the potential energy for these two regimes are listed in Table I. The corresponding diabatic barrier height V_d for these parameters is 1400 cm^{-1} in the normal case, and 1423 cm^{-1} in the inverted regime. For the sake of comparison,

TABLE I. Parameters for the potential energy surface. The range is given for the parameters that are varied. The values of the parameters in brackets are for the inverted regime.

Parameter	Value
ϵ	400 cm^{-1} (12 400 cm^{-1})
V_c	5-1000 cm^{-1}
m_0	1836 a.u.
ω_0	200 cm^{-1}
λ	6374 cm^{-1}
T	575.5 K
η/ω_0	0.1-10

we will use the following classical TST estimate of the rate constant:

$$k_{TST} = \frac{\omega_0}{2\pi} e^{-V_d/k_B T}. \tag{26}$$

For the parameters listed in Table I, $k_{TST} = 0.18$ ps^{-1} in the normal regime.

B. A-FSSH

The algorithm used for A-FSSH dynamics is described in Paper I. The equation of motion for Langevin Eq. (25) is integrated by the method described in Ref. 61 [see Eq. (9.24) therein]. This method is a generalization of the well known velocity-Verlet scheme to include the friction and is known to work well with the FSSH algorithm.[39] Fourth order Runge-Kutta method is used to evolve the quantum amplitudes, and the moments $\delta\mathbf{Q}$, $\delta\mathbf{P}$. The criteria for determining if a trajectory has stabilized in the reactant or the product basin is as follows.

1. In the normal regime, with the reactant towards the left of the curve crossing [see Fig. 1(b)], the trajectory is stabilized in the reactant basin if $Q_0 < Q_{0,r}^{\min}$ (and in the product basin if $Q_0 > Q_{0,p}^{\min}$) and the total energy $E < V_d - k_B T$. Here $Q_{0,r/p}^{\min}$ are the positions at the minimum of the reactant and the product basins, respectively.
2. In the inverted regime, with the upper adiabat representing the reactants [see Fig. 1(c)], the trajectory is stabilized in the reactant basin if $Q_0 > Q_{0,r}^{\min}$ (and in the product basin if $Q_0 > Q_{0,p}^{\min}$) and the total energy $E < V_d - k_B T$.

The direct computation of the rate constant (as discussed in Sec. II A) is performed only for the normal regime. The decay of the population in the reactant well is fit to an exponential. Equation (2) is used to compute the forward rate constant. Given the demanding computational time, an average is taken over 50 000 trajectories for $V_c = 5$ cm^{-1}, 20 000 trajectories for the range $V_c = 10$–100 cm^{-1}, and 2000 trajectories for the range $V_c = 100$–1000 cm^{-1}. A time period ranging from 10 ps to 500 ps is used to perform the exponential fit (except for $V_c = 5$ cm^{-1} for which a linear fit must be performed due to computational cost). The rate constant computed using the much faster TST-like approaches is computed using 50 000 trajectories (for both the normal and the inverted regimes). An integration time step of 0.02 fs is used for all calculations.

C. HEOM

To test the validity of our approaches to compute rate constants, we benchmark our results against the numerically exact HEOM method.[31,33,34,59,62,63] Before we do that, it will be helpful to transform the Hamiltonian given by Eqs. (17)-(23) into a form that is closer to the one generally employed by the HEOM formulation,[60]

$$H = H_s + H_b + H_{sb} + H_{ren}, \tag{27}$$

where

$$H_s = \frac{\epsilon}{2}\sigma_z + V_c\sigma_x, \tag{28}$$

$$H_b = \sum_{i=1}\left(\frac{P_i^2}{2m_i} + \frac{1}{2}m_i\omega_i^2 Q_i^2\right), \tag{29}$$

$$H_{sb} = \sum_{i=1} d_i' Q_i \sigma_z, \tag{30}$$

$$H_{ren} = \sum_{i=1}\frac{d_i'^2}{2m_i\omega_i^2}. \tag{31}$$

Here, the coupling coefficients d_i' are described by the Brownian oscillator spectral density[60]

$$J_B(\omega) \equiv \frac{\pi}{2}\sum_i \frac{d_i'^2}{m_i\omega_i}\delta(\omega - \omega_i), \tag{32}$$

$$= \frac{\lambda}{2}\frac{\omega_0^2\eta\omega}{(\omega^2 - \omega_0^2)^2 + \eta^2\omega^2}, \tag{33}$$

with the reorganization energy λ given by

$$\lambda = \sum_{i=1}\frac{2d_i'^2}{m_i\omega_i^2}. \tag{34}$$

Now, two issues arise in the computation of a rate constant using the HEOM method. The first issue is that the initial bath density matrix used in the HEOM method is at thermal equilibrium, independent of the system. However, the correct initial bath density matrix for Marcus theory must be in equilibrium with the initial diabatic state instead. The second issue is that the implementation of the HEOM method we use — the open-source software PHI[33,34] — employs the Drude spectral density, as opposed to the quantum Brownian oscillator [given by Eq. (32)]. (We note that HEOM calculations have been performed previously for a Brownian spectral density.[64,65] In this paper, we use a Drude spectral density for convenience only.) We resolve both these issues now.

1. Initial density matrix

To resolve the first issue, namely, the fact that the HEOM algorithm always starts with the bath density matrix in thermal equilibrium (independent of the system), we transform coordinates so that the bath is coupled only to the product diabatic state. To this end, consider the transformation

$$Q_i' \equiv Q_i + \frac{d_i'}{m_i\omega_i^2}, \tag{35}$$

and define

$$d_i'' \equiv 2d_i'. \tag{36}$$

Substituting Eqs. (35) and (36) into Eqs. (28)-(31) gives

$$H_s = \frac{\epsilon}{2}\sigma_z + V_c\sigma_x, \tag{37}$$

$$H_b = \sum_{i=1}\left(\frac{P_i^2}{2m_i} + \frac{1}{2}m_i\omega_i^2 Q_i'^2\right), \tag{38}$$

$$H_{sb} = \sum_i d_i'' Q_i' |2\rangle\langle 2|, \tag{39}$$

$$H_{ren} = \sum_{i=1}\frac{d_i''^2}{2m_i\omega_i^2}. \tag{40}$$

Since $d_i'' = 2d_i'$, the coefficients d_i'' are given by the spectral density

$$J_B(\omega) \equiv \frac{\pi}{2}\sum_i \frac{d_i''^2}{m_i\omega_i}\delta(\omega-\omega_i), \tag{41}$$

$$= 2\lambda\frac{\omega_0^2\eta\omega}{(\omega^2-\omega_0^2)^2+\eta^2\omega^2}. \tag{42}$$

Equation (35) has achieved the required transformation: the bath is now coupled only to diabat $|2\rangle$. With this decoupling of the bath modes from diabat $|1\rangle$, the initial density matrix used by HEOM is correct for our purposes.

2. Drude vs. Brownian spectral density

We now turn our attention to the second issue described above. The dynamics for the Hamiltonian given by Eqs. (37)-(42) can be evolved with HEOM (as implemented in PHI) given a Drude spectral density

$$J_D(\omega) = 2\lambda_D\frac{\gamma_D\omega}{\omega^2+\gamma_D^2}, \tag{43}$$

where λ_D is the bath reorganization energy and $1/\gamma_D$ is the bath response time. The Brownian spectral density [given by Eq. (42)] can be identified with the Drude spectral density if $\omega_0 \gg \omega$ and[53]

$$\gamma_D = \frac{\omega_0^2}{\eta}, \tag{44}$$

$$\lambda_D = \lambda. \tag{45}$$

The requirement $\omega_0 \gg \omega$ implies that the system frequency is much greater than the cutoff frequency γ_D of the bath $\omega_0 \gg \gamma_D$. Substituting in Eq. (44) gives

$$\frac{\eta}{\omega_0} \gg 1, \tag{46}$$

so that the Brownian spectral density can be approximated by the Drude spectral density in the strong friction regime.

We have used $\eta/\omega_0 = 10$ for computation of the HEOM rate constants. The rkf45 integrator available in the open-source software PHI[33,34] was employed for these calculations, and the time-local truncation used. Investigating a large range of the diabatic coupling V_c necessitates different fitting procedures for the computation of the different rate constants. For the range V_c = 5–100 cm^{-1}, an exponential fit is performed for the decay of population over 1 ns to obtain the total rate constant k. For this range of V_c, results are obtained with the hierarchy truncation level $K = 300$, and $L_T = 0$ are the number of Matsubara terms included (for the expansion of the Drude spectral density). For the range V_c = 100–1000 cm^{-1}, converged results are obtained with $K = 100$, and $L_T = 1$. An exponential fit is performed for the decay of the population computed until 3 ps giving the total rate constant k. The forward rate constant for all values of V_c is computed using Eq. (2).

D. Straub-Berne theory

Apart from exact HEOM results, SB theory provides another useful point of comparison for surface hopping results.[57] There is an extensive literature on including solvent effects on non-adiabatic processes.[7–10,66–70] SB is a simplified theory of nonadiabatic dynamics with a one-dimensional reaction coordinate (in the normal regime) that assumes all recrossings to be independent, as an extension of the Cline and Wolynes model.[69] Hence, a comparison of SB versus A-FSSH (which accounts for decoherence) as well as versus FSSH (which does not account for decoherence) can help answer: what role does decoherence play in the computation of rate constants?

The transmission coefficient in the SB theory is given by[57]

$$\kappa_{SB}^{-1} = \kappa_{ad}^{-1} + \frac{1-\bar{P}_{LZ}}{2\bar{P}_{LZ}}, \tag{47}$$

where κ_{ad} is the adiabatic (classical) transmission coefficient and $\bar{P}_{LZ}$ is the thermally averaged Landau-Zener (LZ) transition probability

$$P_{LZ} = 1 - \exp\left[-\frac{2\pi V_c^2}{v\hbar F_{12}}\right]. \tag{48}$$

Here, v is a one-dimensional nuclear velocity and F_{12} is the difference of the diabatic slopes at the curve-crossing point. The adiabatic transmission coefficient can be computed using

$$\kappa_{ad} = \frac{\langle\delta(s)v_s h[s(t_P)]\rangle}{\langle\delta(s)v_s h[v_s]\rangle}e^{\beta V_c}, \tag{49}$$

where all dynamics in Eq. (49) are classical, Newtonian mechanics on the ground-state surface. The factor $e^{\beta V_c}$ is introduced to account for the fact that the TST estimate in Eq. (14) is computed in reference to the diabatic barrier height whereas κ_{ad} is an adiabatic transmission coefficient for barrier crossings over the ground state (which should correspond to an adiabatic barrier height). In the diabatic limit, SB theory and Zusman theory[40,66] are identical. An average of 5000 trajectories is used for this computation.

IV. RESULTS

There are several regimes investigated in this paper — normal vs. inverted regimes for the spin-Boson Hamiltonian, diabatic vs. adiabatic regimes (corresponding to the strength of the diabatic coupling), and moderate vs. strong frictional strengths. We now present the results for all these regimes.

A. Normal regime

In this subsection, we assess surface hopping results for the normal spin-Boson Hamiltonian as a function of diabatic coupling and frictional strength.

1. Transition state regime (dynamics with no friction)

Our first task is to validate surface hopping by comparison with Marcus theory. In the weak diabatic coupling regime[71]

$$\kappa_M^d = \frac{2\pi\sqrt{\pi}V_c^2}{\hbar\omega_0\sqrt{\lambda k_B T}} \tag{50}$$

and in the adiabatic regime (when the diabatic coupling (V_c) is large), the TST estimate is

$$\kappa_M^{ad} = e^{V_c/k_B T}. \tag{51}$$

Marcus theory presumes that friction is strong enough to maintain a thermal equilibrium of positive velocities at the transition state, but there are no re-crossings (i.e., zero friction); these are, of course, the assumptions for which TST yields the exact classical rate. To simulate this regime, the damping parameter η is set to zero, and the trajectories are considered to be stabilized in the reactant or the product region if they reach the respective minima. The initial distribution of velocity is chosen from a Maxwell-Boltzmann distribution. The results shown in Fig. 2 exhibit a smooth transition from the diabatic limit to the adiabatic limit.[72]

We can highlight the importance of the appropriate treatment of decoherence and frustrated hops by performing two separate calculations — one where the quantum amplitudes do not collapse and one where the velocities are not reversed upon encountering frustrated hops. We discuss the latter issue in Sec. V. The results obtained without any decoherence are labelled as FSSH in Fig. 2. Note that FSSH rate constants are smaller than the A-FSSH rate constants in the diabatic regime. As was highlighted in Paper I, this discrepancy is easily explained by considering those trajectories that hop to the upper adiabat. In the absence of decoherence, such trajectories can effectively never switch diabats and thus one ignores all dynamical effects that can lead to transmission via the upper adiabat. Thus, we expect the FSSH rate to be smaller by about a factor of 2 since only the trajectories that never switch adiabats transmit.[35] As an aside, it is interesting that, for the choice of parameters in this paper, including decoherence increases the FSSH rate of decay whereas, in previous papers, we have shown that including decoherence dramatically reduces the rate of decay (assuming a direct calculation with a stronger driving force).[28,29,40,53]

In the adiabatic regime, the dynamics on the upper surface is less important, and hence there is little difference between the A-FSSH and the FSSH results.

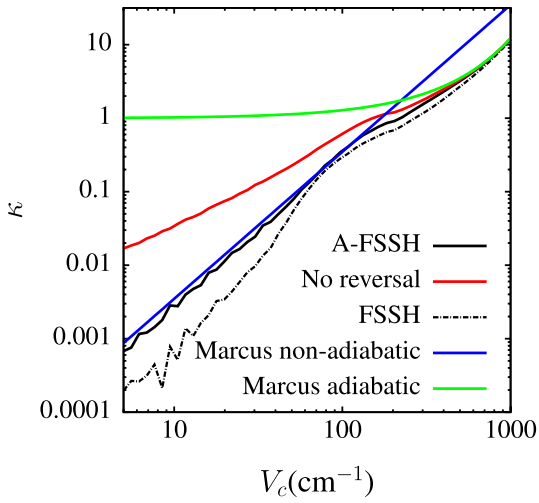

FIG. 2. The transmission coefficient as a function of the diabatic coupling V_c in the case that there is no friction after the crossing point. Note that the transmission coefficient is defined from Eq. (15) and thus can be larger than 1. Here, we compare two versions of surface hopping, A-FSSH (with decoherence) and FSSH (without decoherence) versus diabatic [Eq. (50)] and adiabatic [Eq. (51)] Marcus theory. The TST rate constant in Eq. (14) is $k_{TST} = 0.18$ ps^{-1}. Both A-FSSH and FSSH correctly interpolate from the diabatic to the adiabatic limits of TST theory as V_c increases. In the diabatic regime (small V_c), FSSH underestimates the transmission coefficient due to an incorrect treatment of dynamics on the upper adiabat. This figure also demonstrates (in red) the importance of correct treatment of the frustrated hops, particularly in the diabatic regime.

2. Strong friction regime

Our second task is to analyze κ in the strong friction regime ($\eta/\omega_0 = 10$) where numerically exact HEOM rate constants are available. Figure 3 shows the results. We compare rate constants from A-FSSH, FSSH, HEOM and SB dynamics. We also study A-FSSH dynamics as computed from a direct, brute-force calculation. As one would hope, the transmission coefficient from all of these different approaches are rather similar across a broad range of diabatic couplings. As in the case of no friction, FSSH rate constants are smaller than A-FSSH rate constants in the diabatic limit; however, the difference is not as dramatic in this case, as the strong coupling with the bath leads to increased re-crossings. The biggest difference between the A-FSSH results and the HEOM results occur near $V_c \sim 1000$ cm^{-1}. In this adiabatic regime, however, the barrier

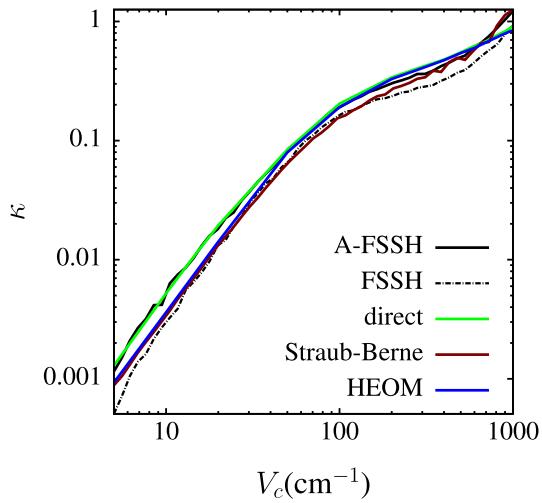

FIG. 3. The transmission coefficient as a function of the diabatic coupling V_c in the strong friction regime $\eta/\omega_0 = 10$. We provide comparisons of A-FSSH-TST results with direct A-FSSH dynamics, exact HEOM results, FSSH-TST results, and SB theory. A-FSSH results compare well with the HEOM results across a broad regime of diabatic couplings.

height is only 400 cm^{-1}, which is equal to k_BT. Since TST relies on the assumption of barrier height being much larger than k_BT, TST is likely not applicable for such large values of V_c.

In the strong friction regime, not reversing velocities upon encountering a frustrated hop has insignificant effects, as will be discussed in greater detail in Sec. V

3. Frictional dependence

Our third task is to investigate the effect of frictional strength η on the transmission coefficient. Figure 4 shows a comparison of κ from A-FSSH vs. κ from SB theory as a function of the dimensionless friction parameter η/ω_0 for two different values of V_c. The figure shows results for both the forward (left → right) and reverse (right → left) reactions. For small diabatic couplings (V_c = 20 cm^{-1}), we observe a broad region where κ is relatively independent of friction strength, in excellent agreement with the predictions of the SB theory. That being said, upon close inspection of this figure, one can notice a small increase in κ from 0.014 to 0.018 as η/ω_0 varies from 0.1 to 10 for V_c = 20 cm^{-1}. We believe this non-physical increase can be interpreted as corresponding to a weak correlation between the number of frustrated hops and the strength of the friction.[73]

Finally, in Fig. 4, we also plot (in green) κ as obtained without reversing velocities (see Sec. II C 3) on encountering a frustrated hop; this curve will be discussed in greater detail in Sec. V.

B. Inverted regime

Next, we turn our attention to the inverted regime. We compare results only in the weak coupling regime—at large V_c, the reactant and product basins start mixing and TST is inapplicable. As discussed in Sec. II D, in practice, when computing rate constants for the normal regime vs. the inverted regime, the only change required in the algorithm is a change in identification of the reactant basin and the product basin. These identifications are necessary both (i) for determining if a trajectory has stabilized in the reactant or product basin at long times and (ii) for choosing the adiabatic surface necessary for backward propagation towards the reactants.

Figure 5 shows good agreement between the A-FSSH results with the Marcus estimate [see Eq. (50)] in the zero frictional regime, and good agreement with HEOM results in the strong friction regime. We have also plotted the forward and the backward rate constants, and their near agreement is encouraging. Overall, these results indicate that a TST-AFSSH algorithm can be robust and accurate across various regimes — normal and the inverted regimes, small to large diabatic couplings, and moderate to strong frictional strengths.

V. DISCUSSION

Having investigated surface hopping rate constants across many different regimes, we now discuss several important issues that merit comment: detailed balance, choice of dividing surface, velocity reversal, and local temperature.

A. Detailed balance

To assess whether or not detailed balance is satisfied by the A-FSSH algorithm, we have computed backward transmission coefficients for every single calculation where a forward transmission coefficient has been computed. As an example, see Figs. 4 and 5. For all such calculations, we find that the forward and the backward transmission coefficients match extremely well for the normal case, while there are minor differences in the inverted regime. This approximate equivalence between transmission coefficients implies automatically that detailed balance will be satisfied approximately.

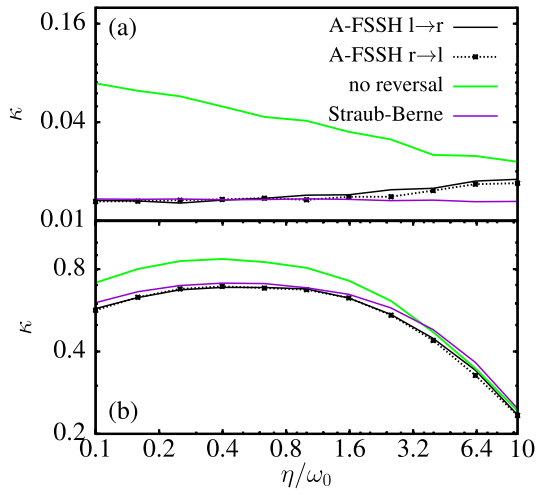

FIG. 4. The transmission coefficient computed using A-FSSH as a function of the dimensionless friction strength η/ω_0. (a) V_c = 20 cm^{-1} and (b) V_c = 200 cm^{-1}. SB theory generally agrees well with A-FSSH results. Note the small unphysical increase in κ computed using A-FSSH for V_c = 20 cm^{-1}, which we believe is due to the decreasing number of frustrated hops over the friction regime. Also note that, for the case V_c = 20 cm^{-1}, much larger results are obtained if velocities are not reversed on encountering a frustrated hop.

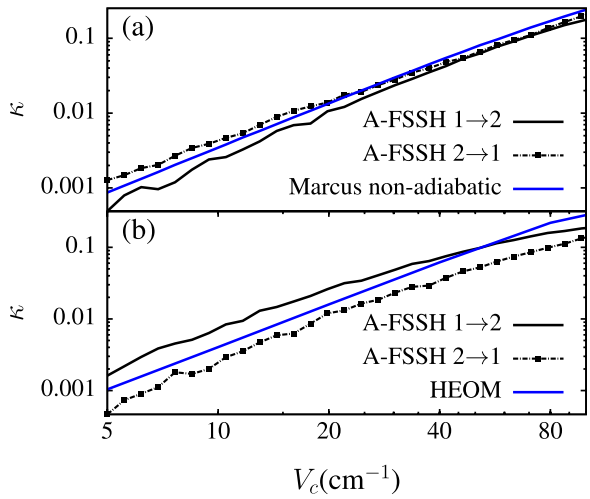

FIG. 5. The transmission coefficient as a function of the diabatic coupling V_c for the inverted potential (see Fig. 1(c)). (a) No friction and (b) strong friction (η/ω_0 = 10). A-FSSH results compare well against nonadiabatic Marcus theory [Eq. (50)] and HEOM results in the two frictional regimes. The forward and the backward transmission coefficients have relatively minor differences.

Now, detailed balance is sometimes interpreted as a consequence of time-reversibility.[36] And one should recall that, according to Paper I, time-reversibility is not obeyed exactly by A-FSSH dynamics — the forward and the backward transmission factors oscillate at different frequencies for trajectories in a microcanonical ensemble. Thus, without knowledge of the Schmidt/Parandekhar/Tully papers,[38,41] one might not expect surface hopping to recover detailed balance. However, we must emphasize that, in Paper I, we showed that, after averaging over energy to wash away any oscillations in transmission factors, one finds nearly identical probabilities of transmission for forward and reverse scattering quantum wavepackets. We now see that this gas-phase conclusion holds in the condensed phase as well.

B. Initial choice of the dividing surface

Let us now discuss the choice of dividing surface. An exact quantum or classical rate theory is always independent of the choice of dividing surface. For a mixed quantum-classical theory, we can certainly not hope for complete independence, but we do require an approximate TST scheme to be approximately invariant to dividing surface if the scheme is to be useful. In Paper I, we showed that scattering transmission probabilities (in one dimension) can be computed over a broad range of dividing surfaces with little error. We would now like to check whether this robustness is preserved when computing rate constants.

To probe this last statement, we vary the starting point in the algorithm above (Sec. II D) for $V_c = 20$ cm^{-1}. We compare results from Eq. (15) versus results using a Boltzmann average of the contributions of the two adiabats (as suggested by Hammes-Schiffer and Tully in Ref. 16),

$$\kappa^B = \frac{\sum_j \langle \delta(s) v_s h[v_s] \alpha \rangle_j}{\langle \delta(s) v_s h[v_s] \rangle_d}, \tag{52}$$

with

$$\langle (\ldots) \rangle_j = \frac{1}{Z} \int d\mathbf{P} e^{-\beta \sum_i P_i^2/2m_i} \int d\mathbf{Q} e^{-\beta V_j(\mathbf{Q})} (\ldots). \tag{53}$$

Here, j represents the surface on which the trajectory is initiated for the forward propagation. $\langle (\ldots) \rangle_d$ is defined in Eq. (16).

Figure 6 shows the left to right transmission coefficients in the normal regime as a function of δQ (which is defined as the difference between the dividing surface chosen and the location of the diabatic curve crossing ($Q^\ddagger$)). Clearly, the results obtained with Eq. (15) are relatively independent of the choice of the dividing surface. In the zero-friction regime, there are small oscillations for positive δQ, which are presumably a result of constructive and destructive interferences. By contrast, for a Boltzmann average [see Eq. (52)], the transmission coefficient changes by a factor of roughly 0.5 for large positive δQ. This factor of 0.5 arises because the contribution to κ from the upper adiabat gets a very small weight, effectively giving similar results as that of FSSH. (See Fig. 2 for a different perspective on the same factor of 1/2.) Although this factor of 1/2 arises using our simplified scheme of backward propagation, the HST algorithm of Ref. 16 should give results that are close to independent of the dividing surface.[24]

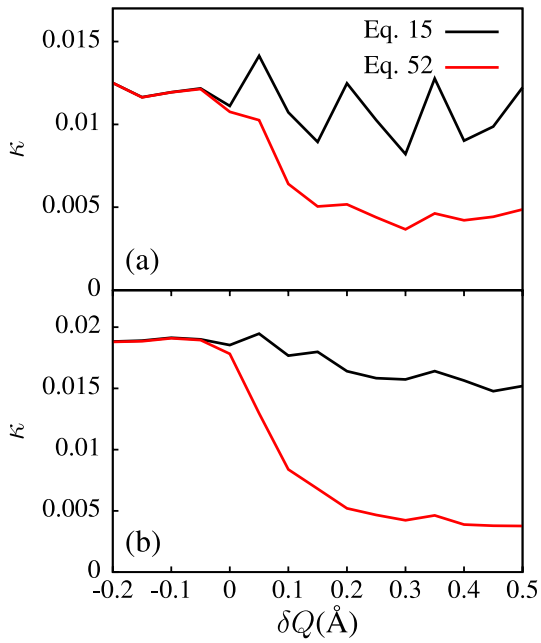

FIG. 6. The variation of the transmission coefficient as a function of the location of the dividing surface. The x-axis δQ denotes the difference between the dividing surface and the true curve crossing. The results are shown for the normal reaction for (a) zero friction and (b) strong friction ($\eta/\omega_0 = 10$). The results obtained with Eq. (15) are relatively independent of the dividing surface, while results obtained with Eq. (52) are not.

Figure 7 shows the top to bottom transmission coefficients as a function of δQ for the inverted regime. In this regime, for negative δQ, the population flux decreases, leading to smaller rate constants, as can be seen easily with Eq. (15). From our perspective, this decrease is inevitable. From a practical view,

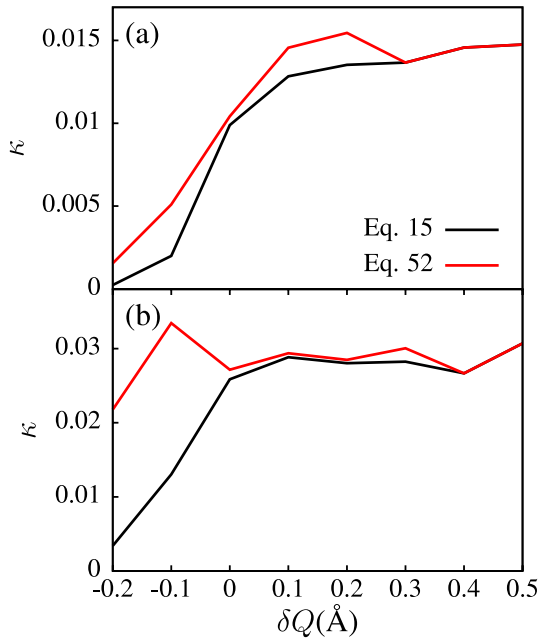

FIG. 7. Same as in Fig. 6, but in the inverted regime. The results are relatively independent of the location of the dividing surface if the dividing surface is chosen to the right of the curve-crossing ($\delta Q > 0$).

trajectories that cross between diabats need only to reach the crossing point to hop in the inverted regime. With that in mind, we study the more important case — when δQ is positive. In this case, the results are relatively independent of the choice of the dividing surface and the Boltzmann averaging gives similar results to that of Eq. (15). This invariance is encouraging.

C. Frustrated hops and velocity reversal

To assess the effect of forbidden hops on thermally activated rare event processes, in Figs. 2 and 4, we have computed and compared κ both with and without velocity reversals (after a forbidden hop). The results are clear. Without velocity reversal, the computed κ can be much larger than exact results. With velocity reversal, however, A-FSSH dynamics can be very accurate. We believe this conclusion should be a resounding endorsement of some minimal form of velocity reversal (we are using a slightly more constrained version of the Jasper/Truhlar scheme).[48]

Let us further investigate Figs. 2 and 4. Upon inspection, we find that frustrated hops make a dramatic difference only when (i) the coupling to the bath is in the weak to moderate frictional regime and (ii) the diabatic coupling is small. These findings are straightforward to understand. (i) In the regime of strong friction strength, the inertia (preventing ballistic transport) provides more opportunities for the trajectory to hop successfully and reversing the velocity at time $t = 0$ has a minimal effect at later times. (ii) In the large coupling (adiabatic) regime (in the normal regime), motion is predominantly along the lower adiabat and contributions due to frustrated hops are not significant.

Now, if one assumes weak friction, one can calculate an upper bound for the error in transmission probability that arises from not reversing velocities after a forbidden hop. Assume that all trajectories with energy between 0 and $2V_c$ transmit. Then, the potentially spurious probability of transmission will be bounded by

$$\bar{P}_{LZ}^{fr} = \frac{\int_0^{2V_c} dE e^{-\beta E}}{\int_0^{\infty} dE e^{-\beta E}}, \tag{54}$$

$$= 1 - e^{-\beta 2V_c}, \tag{55}$$

$$\sim \beta 2V_c. \tag{56}$$

In the last equation, the diabatic limit is taken ($V_c \to 0$). Note that Eq. (56) varies linearly with V_c. For frustrated hops to significantly alter our surface hopping results, the probability above must be much larger than the nonadiabatic Marcus estimate,

$$\beta 2V_c \gg \frac{2\pi\sqrt{\pi}V_c^2}{\hbar\omega_0\sqrt{\lambda k_B T}}. \tag{57}$$

Simplifying,

$$V_c \ll \frac{\hbar\omega_0}{\pi\sqrt{\pi}}\sqrt{\frac{\lambda}{k_B T}}. \tag{58}$$

For the parameters in the normal regime (Table I), this condition is $V_c \ll 140$ cm^{-1}; indeed, in Fig. 2, the red and black curves coincide for $V_c > 140$. Similar reasoning can perhaps be useful in predicting scenarios where frustrated hops would play an important role for a general system undergoing a rare event crossing.

D. Thermal distribution at the transition state

Another point of interest is the question of how to initialize velocities. Thus far, in this paper, all results have been computed using an uncorrelated protocol [see Eq. (13)], whereby one assumes that the velocities at the transition state should be sampled from the same Boltzmann distribution on both of the two adiabatic surfaces (as usually done in TST, e.g., in the HST approach).[16] In contrast to this protocol, in Paper I, for gas-phase scattering calculations, the nuclear velocities at the transition state were initialized from a Boltzmann distribution on the lower surface, but from a different distribution on the upper surface (corresponding to the reduced velocities what one would obtain after an upwards surface hop). The two protocols just described can be labeled "uncorrelated" and "correlated," respectively.

In our numerical studies to date, both these initialization protocols give near identical results for all the regimes investigated, provided that the dividing surface coincides with the curve-crossing location. However, the different initialization protocols do make a significant difference when the dividing surface is changed. On the one hand, if initial velocities are chosen independently, the results are approximately independent of the choice of the dividing surface. On the other hand, correlated initialization protocol leads to dramatically larger results for positive δx (in the normal regime), since a large number of trajectories are initially frustrated (i.e., they are chosen to be initiated on the upper surface but do not have energy to do so) and transmit with forward propagation (not shown in Fig. 6).

To further justify this assumption of uncorrelated initial velocities, we have also performed an explicit test to see if the velocities have the same or different distributions at the transition state. To this end, we evolve 3000 trajectories for very long times (0.5 ns, each initiated at the reactant and equilibrated for 50 ps, with an integration time step of 0.02 fs) and compute the temperature on the two surfaces as $k_B T_i = \langle m v_i^2 \rangle$. Here, v_i is the velocity for the trajectories on the two adiabats at the curve-crossing. The transition state is identified as $|Q_0 - Q_0^{\ddagger}| < 0.01$ Å. Small variations to the bin size of 0.01 Å do not make any appreciable difference.

Figure 8 shows the computed temperatures at the crossing point as a function of friction strength for $V_c = 200$ cm^{-1} and $k_B T = 400$ cm^{-1}. In the strong friction regime, the temperatures are the same as the temperature of the bath, as expected. In the low friction regime ($\eta/\omega \sim 0.1$), the velocity temperature is smaller for the upper adiabat. This reduction must be a consequence of the velocity rescaling that occurs upon surface hopping upwards. The moderate friction regime ($\eta/\omega \sim 1$) presents a surprising result in so far that the upper surface now has a higher temperature than the lower surface. Two possible reasons for this increase are (1) frustrated hops favor lower velocities remaining on the ground surface and (2) trajectories with higher velocities are more likely to hop up. These two effects compete with the velocity rescaling at low frictions, giving the interesting frictional dependence in Fig. 8.

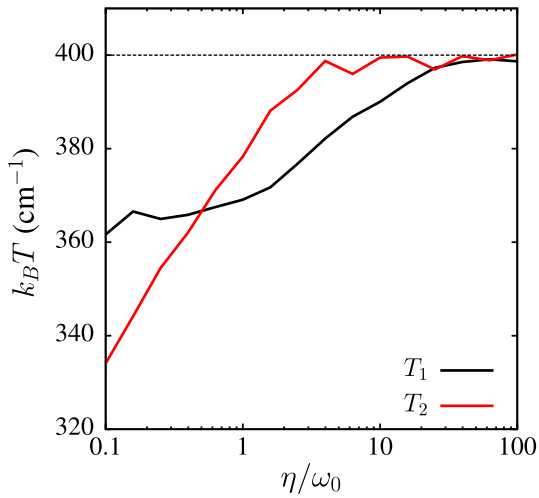

FIG. 8. The temperature on the two surfaces at the crossing point as a function of the friction strength. Here, the temperature is defined by $k_BT_i = \langle mv_i^2 \rangle$, where i refers to the adiabatic surface for which the temperature is computed. The physical temperature is $k_BT = 400$ cm^{-1} (dotted line).

Notwithstanding these differences, however, the reader should note the temperature scale of the Fig. 8: the temperatures of the two surfaces are not that different. Thus, we believe initializing velocities from an uncorrelated distribution is a workable approximation.

E. Variation of temperature with nuclear position

The final questions we address regard the notion of local temperature. These questions come in two forms. First, how does the nuclear velocity distribution depend on position? This dependence is a very important consideration since, in Eq. (13), we assume a Boltzmann distribution of initial velocities, independent of the position of the dividing surface. To date, no one has shown whether or not the velocities are indeed thermally equilibrated at the temperature of the thermal bath for all positions near a crossing point. We now test this proposition numerically, following the procedure described in Sec. V D. Second, do the equilibrium populations on the two adiabats satisfy detailed balance as a function of the position of the dividing surface? These populations are important for the HST scheme.[16,17]

To answer both these issues, we define two different measures of temperature — the velocity temperature on the two adiabats i as

$$k_BT_i^v = \langle mv_i^2 \rangle, \tag{59}$$

and the population temperature

$$k_BT^p(Q_0) = \frac{V_2(Q_0) - V_1(Q_0)}{-\ln(p_2/p_1)}, \tag{60}$$

where p_i are the populations on the two adiabats.

Figure 9 shows the temperatures as a function of $\delta Q = Q_0 - Q_0^\ddagger$ (where $Q_0^\ddagger$ is the transition state value). The velocity temperatures are very close to the bath thermal temperature of 400 cm^{-1} (except for a small dip of the ground state velocity temperature near the curve crossing). This suggests that choosing initial velocities from a Boltzmann distribution, independent of the dividing surface is a good approximation.

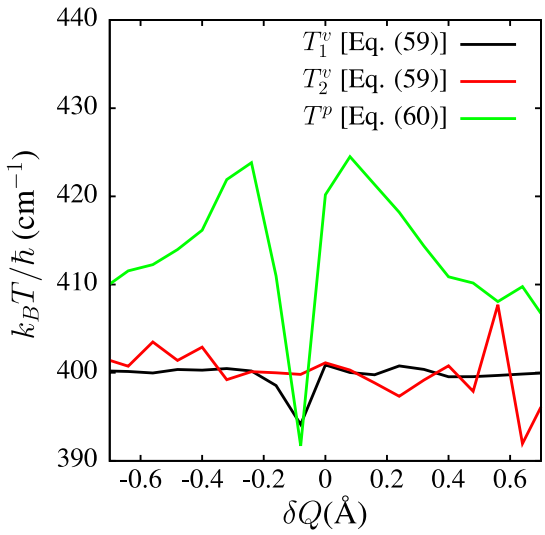

FIG. 9. The temperature on the two surfaces as a function of the position δQ (with respect to the transition state) as measured by nuclear velocities [T^v, see Eq. (59)] and electronic populations [T^p, see Eq. (60)]. The physical temperature is $k_BT = 400$ cm^{-1}.

The population temperatures are slightly higher (by about 10 cm^{-1}) than the bath temperature away from the curve-crossing and exhibits a sharp dip at the curve-crossing. The scale of these deviations appears reasonably minor, however, and unlikely to affect the HST algorithm significantly.

VI. SUMMARY AND CONCLUSIONS

We have investigated a modified TST-FSSH scheme over a broad range of parameter regimes, using a scheme similar to the Hammes-Schiffer and Tully's algorithm.[16] We have explored a wide range of diabatic couplings and friction strengths for both the normal and the inverted case of the spin-Boson Hamiltonian and have compared transmission coefficients with numerically exact HEOM results. In response to our objectives presented in the Introduction, our specific conclusions are as follows.

1. Our TST-AFSSH results compare well with direct computation, as well as HEOM.
2. Our modified TST-AFSSH protocol gives results that are approximately independent of the choice of the dividing surface (within reason). We expect this approximate independence to hold quite generally, as the underlying reason for this independence is also behind the independence of the classical rate constant — all the trajectories are weighted by the ground adiabatic surface. At steady state, approximating excited state populations dynamically (using $|c_j|^2$) would appear robust.
3. The A-FSSH algorithm obeys detailed balance approximately. All of the computed thermally averaged forward and backward transmission coefficients are close.
4. Without any decoherence, surface hopping rate constants can be somewhat incorrect in the diabatic regime.
5. An incorrect treatment of frustrated hops can lead to much larger rate constants in the limit of small friction and small diabatic couplings. We have obtained encouraging results with reversing the velocities along the non-adiabatic

coupling vector on encountering a frustrated hop. Without such a velocity reversal, the rate constants can be several orders of magnitude larger. It remains to be tested if this velocity reversal scheme works for more complicated potential energy surfaces.

6. We have shown that in order to attain a rate constant that is reasonably insensitive to dividing surface using our Markovian scheme, it is essential that we choose the initial set of nuclear velocities to be sampled from a Boltzmann distribution and entirely decoupled from (and independent of) the identity of the electronic state and the nuclear position.

Overall, with proper treatment of decoherence and frustrated hops, we find that a surface hopping can be matched up well with TST. Our next step forward now is to apply the methods discussed here to large, multidimensional systems, where a direct application of surface hopping may be too time-consuming and questions of decoherence are outstanding.

ACKNOWLEDGMENTS

This material is based upon work supported by the (U.S.) Air Force Office of Scientific Research (USAFOSR) PECASE award under AFOSR Grant No. FA9950-13-1-0157. J.E.S. acknowledges a Cottrell Research Scholar Fellowship and a David and Lucille Packard Fellowship.

[1]R. Marcus, Annu. Rev. Phys. Chem. **15**, 155 (1964).
[2]N. L. Doltsinis, "Nonadiabatic dynamics: Mean-field and surface hopping," in *Quantum Simulations of Complex Many-Body Systems: From Theory to Algorithms*, edited by J. Grotendorst, D. Marx, and A. Muramatsu (NIC, FZ Julich, 2002), www.fz-juelich.de/nic-series/volume10/doltsinis.pdf.
[3]J. C. Tully, J. Chem. Phys. **93**, 1061 (1990).
[4]S. Hammes-Schiffer and J. C. Tully, J. Chem. Phys. **101**, 4657 (1994).
[5]U. Müller and G. Stock, J. Chem. Phys. **107**, 6230 (1997).
[6]M. Barbatti, WIREs: Comput. Mol. Sci. **1**, 620 (2011).
[7]J. T. Hynes, Annu. Rev. Phys. Chem. **36**, 573 (1985).
[8]B. J. Berne, M. Borkovec, and J. E. Straub, J. Phys. Chem. **92**, 3711 (1988).
[9]P. Hänggi, P. Talkner, and M. Borkovec, Rev. Mod. Phys. **62**, 251 (1990).
[10]E. Pollak and P. Talkner, Chaos **15**, 026116 (2005).
[11]W. H. Miller, J. Chem. Phys. **61**, 1823 (1974).
[12]W. H. Miller, S. D. Schwartz, and J. W. Tromp, J. Chem. Phys. **79**, 4889 (1983).
[13]A. Warshel and J.-K. Hwang, J. Chem. Phys. **84**, 4938 (1986).
[14]R. Kapral, Annu. Rev. Phys. Chem. **57**, 129 (2006).
[15]R. Kapral, J. Phys.: Condens. Matter **27**, 073201 (2015).
[16]S. Hammes-Schiffer and J. C. Tully, J. Chem. Phys. **103**, 8528 (1995).
[17]S. R. Billeter, S. P. Webb, T. Iordanov, P. K. Agarwal, and S. Hammes-Schiffer, J. Chem. Phys. **114**, 6925 (2001).
[18]P. K. Agarwal, S. R. Billeter, P. T. R. Rajagopalan, S. J. Benkovic, and S. Hammes-Schiffer, Proc. Natl. Acad. Sci. U. S. A. **99**, 2794 (2002).
[19]P. K. Agarwal, S. R. Billeter, and S. Hammes-Schiffer, J. Phys. Chem. B **106**, 3283 (2002).
[20]J. B. Watney, P. K. Agarwal, and S. Hammes-Schiffer, J. Am. Chem. Soc. **125**, 3745 (2003).
[21]S. Y. Kim and S. Hammes-Schiffer, J. Chem. Phys. **124**, 244102 (2006).
[22]S. Hammes-Schiffer, Acc. Chem. Res. **39**, 93 (2006).
[23]V. C. Nashine, S. Hammes-Schiffer, and S. J. Benkovic, J. Curr. Opin. Chem. Biol. **14**, 644 (2010).
[24]C. A. Schwerdtfeger, A. V. Soudackov, and S. Hammes-Schiffer, J. Chem. Phys. **140**, 034113 (2014).
[25]B. J. Schwartz, E. R. Bittner, O. V. Prezhdo, and P. J. Rossky, J. Chem. Phys. **104**, 5942 (1996).
[26]M. J. Bedard-Hearn, R. E. Larsen, and B. J. Schwartz, J. Chem. Phys. **123**, 234106 (2005).
[27]G. Granucci, M. Persico, and A. Zoccante, J. Chem. Phys. **133**, 134111 (2010).
[28]B. R. Landry and J. E. Subotnik, J. Chem. Phys. **135**, 191101 (2011).
[29]B. R. Landry and J. E. Subotnik, J. Chem. Phys. **137**, 22A513 (2012).
[30]J. E. Subotnik, W. Ouyang, and B. R. Landry, J. Chem. Phys. **139**, 214107 (2013).
[31]A. Ishizaki and Y. Tanimura, J. Phys. Soc. Jpn. **74**, 3131 (2005).
[32]A. Ishizaki and G. R. Fleming, J. Chem. Phys. **130**, 234111 (2009).
[33]J. Strmpfer and K. Schulten, J. Chem. Phys. **131**, 225101 (2009).
[34]J. Strmpfer and K. Schulten, J. Chem. Theory Comput. **8**, 2808 (2012).
[35]A. Jain, M. F. Herman, W. Ouyang, and J. Subotnik, "Surface hopping, transition state theory and decoherence. I. Scattering theory and time-reversibility," J. Chem. Phys. **143**, 134106 (2015).
[36]B. H. Mahan, J. Chem. Educ. **52**, 299 (1975).
[37]J. E. Subotnik and Y. M. Rhee, J. Phys. Chem. A **119**, 990 (2015).
[38]J. R. Schmidt, P. V. Parandekar, and J. C. Tully, J. Chem. Phys. **129**, 044104 (2008).
[39]M. C. Sherman and S. A. Corcelli, J. Chem. Phys. **142**, 024110 (2015).
[40]M. J. Falk, B. R. Landry, and J. E. Subotnik, J. Phys. Chem. B **118**, 8108 (2014).
[41]P. V. Parandekar and J. C. Tully, J. Chem. Phys. **122**, 094102 (2005).
[42]J.-Y. Fang and S. Hammes-Schiffer, J. Chem. Phys. **110**, 11166 (1999).
[43]C. Zhu, K. Nobusada, and H. Nakamura, J. Chem. Phys. **115**, 3031 (2001).
[44]P. Oloyede, G. Milnikov, and H. Nakamura, J. Chem. Phys. **124**, 144110 (2006).
[45]M. F. Herman, Chem. Phys. **433**, 12 (2014).
[46]A. W. Jasper, M. D. Hack, and D. G. Truhlar, J. Chem. Phys. **115**, 1804 (2001).
[47]A. W. Jasper, S. N. Stechmann, and D. G. Truhlar, J. Chem. Phys. **116**, 5424 (2002).
[48]A. W. Jasper and D. G. Truhlar, Chem. Phys. Lett. **369**, 60 (2003).
[49]A. W. Jasper and D. G. Truhlar, J. Chem. Phys. **127**, 194306 (2007).
[50]Y. Zhao, X. Li, Z. Zheng, and W. Liang, J. Chem. Phys. **124**, 114508 (2006).
[51]C. Zhu and H. Nakamura, J. Chem. Phys. **101**, 10630 (1994).
[52]Y. Zhao, M. Han, W. Liang, and H. Nakamura, J. Phys. Chem. A **111**, 2047 (2007).
[53]B. R. Landry and J. E. Subotnik, J. Chem. Phys. **142**, 104102 (2015).
[54]W. Xie, S. Bai, L. Zhu, and Q. Shi, J. Phys. Chem. A **117**, 6196 (2013).
[55]D. Chandler, *Introduction to Modern Statistical Mechanics* (Oxford University Press, 1987).
[56]J. Keck, Discuss. Faraday **33**, 173 (1962).
[57]J. E. Straub and B. J. Berne, J. Chem. Phys. **87**, 6111 (1987).
[58]A. Sergi and R. Kapral, J. Chem. Phys. **118**, 8566 (2003).
[59]Q. Shi, L. Chen, G. Nan, R. Xu, and Y. Yan, J. Chem. Phys. **130**, 164518 (2009).
[60]A. Garg, J. N. Onuchic, and V. Ambegaokar, J. Chem. Phys. **83**, 4491 (1985).
[61]M. P. Allen and D. J. Tildesley, *Computer Simulation of Liquids* (Clarendon Press, New York, NY, USA, 1989).
[62]Y. Tanimura and R. Kubo, J. Phys. Soc. Jpn. **58**, 1199 (1989).
[63]Y. Tanimura, J. Phys. Soc. Jpn. **75**, 082001 (2006).
[64]M. Tanaka and Y. Tanimura, J. Chem. Phys. **132**, 214502 (2010).
[65]L. Zhu, H. Liu, W. Xie, and Q. Shi, J. Chem. Phys. **137**, 194106 (2012).
[66]L. Zusman, Chem. Phys. **49**, 295 (1980).
[67]P. G. Wolynes, Phys. Rev. Lett. **47**, 968 (1981).
[68]I. Rips and J. Jortner, J. Chem. Phys. **87**, 2090 (1987).
[69]R. E. Cline and P. G. Wolynes, J. Chem. Phys. **86**, 3836 (1987).
[70]J. N. Onuchic and P. G. Wolynes, J. Phys. Chem. **92**, 6495 (1988).
[71]A. Nitzan, *Chemical Dynamics in Condensed Phases: Relaxation, Transfer and Reactions in Condensed Molecular Systems: Relaxation, Transfer and Reactions in Condensed Molecular Systems* (Oxford University Press, Great Clarendon Street, Oxford OX2 6DP, United Kingdom, 2006).
[72]P. Huo, T. F. Miller III, and D. F. Coker, J. Chem. Phys. **139**, 151103 (2013).
[73]In our simulations, we kept statistics of the number of frustrated hops that each trajectory experiences on average. Interestingly, as η/ω_0 varies from 0.1 to 10, the spurious percentage increase in the transmission coefficient correlates very well with a relative decrease in the number of frustrated hops (and thus less velocity reversals). This correlation is observed for the diabatic coupling strengths in the range 5-50 cm^{-1} and might offer one explanation for the small spurious increase of κ in Fig. 4.